

What Determines Electrochemical Surface Processes on Carbon-Supported PdAu Nanoparticles?

Irã B. C. Gallo¹, Emilia A. Carbonio², Hebe M. Villullas^{1}*

1. Universidade Estadual Paulista (UNESP), Instituto de Química, Araraquara, 14800-060

Araraquara (SP), Brazil.

2. Helmholtz-Zentrum Berlin für Materialien und Energie, BESSY-II, Albert-Einstein-Straße 15,

12489, Berlin, Germany.

ABSTRACT. Supported bimetallic nanoparticles have good activities in heterogeneous catalysis and electrocatalysts. Among those systems, PdAu shows improved stability and enhanced catalytic activity towards electrochemical reactions such as oxygen reduction, formic acid oxidation and hydrogen evolution. The aim of this work was to study comprehensively the influence of ligand and ensemble effects on surface processes, such as oxide formation/reduction, oxidation of adsorbed CO and adsorption of hydrogen, taking place on carbon-supported PdAu nanoparticles of different compositions. Towards that end, we thoroughly characterized the properties of PdAu/C catalysts with nominal Au contents of 20 to 50 % (in atoms) prepared by the same procedure and having similar average particle diameters. The combination of results obtained by X-ray diffraction (XRD) and X-ray photoelectron spectroscopy (XPS) indicates that nanoparticles had Pd-enriched surfaces and Au-rich interior. X-ray absorption spectroscopy (XAS) measurements around the Pd L3 edge evidenced that Au promotes an increase in the electronic occupation of the Pd 4d band, consistent with XPS results showing varying amounts of surface-like and bulk-like Pd oxide and

*Corresponding author: mercedes@iq.unesp.br

metallic Pd. We show herein that ligand effects determine the formation of a Pd oxide layer on PdAu/C catalysts and ensemble effects govern hydrogen and CO adsorption. CO oxidation is delayed as the Au content increases as result of the decreasing availability of oxygen-containing species.

KEYWORDS: Bimetallic nanoparticles; Ligand effects, Ensemble effects, Oxide formation/reduction; CO oxidation; Hydrogen adsorption.

INTRODUCTION

The distinctive properties of bimetallic systems, which often result in significantly enhanced catalytic activities as compared to the individual components, have an undeniable relevance in heterogeneous catalysis.¹ Bimetallic nanoparticles are also very relevant in electrocatalysis, mainly regarding fuel cell reactions²⁻⁴ and other energy-related processes, such as hydrogen evolution.⁵ Even though over the last decades research devoted to develop fuel cell catalysts was mainly focused on Pt-based nanoparticles,³ Pd and Pd-based nanocatalysts attracted increasing attention as feasible and cheaper substitutes for Pt in fuel cell cathodes and as alcohol tolerant catalysts in acidic environments.⁶ Consequently, the activities of Pd-based bimetallic systems involving a variety of other metals, such as Ni, Fe, Co, etc. were studied and the main findings can be found in recent reviews.^{5,7} Pd is an active catalyst for a variety of chemical and electrochemical reactions, but lacks stability under corrosive environments. Au is not as active as electrocatalyst, but its good stability can help to stabilize other metals. For instance, Pt nanoparticles modified with Au clusters were found to be more stable against dissolution in oxygen reduction conditions.⁸ Consequently, the considerable attention received by PdAu catalysts results from the possibility

of combining the good catalytic activity of Pd with improved stability provided by Au. Published results demonstrate that the PdAu system exhibits good activity for a number of chemical processes of industrial and environmental importance.⁹⁻¹³ Literature results also revealed good activities of PdAu thin layers for hydrogen evolution and oxidation,¹⁴ and enhanced electrocatalytic activities of carbon-supported PdAu nanoparticles for reactions relevant to fuel cell development, such as oxygen reduction¹⁵⁻¹⁹ and formic acid oxidation.²⁰⁻²¹ Improved CO tolerance of carbon-supported PdAu catalysts has also been reported.²²

Catalytic enhancements promoted by bimetallic systems are usually associated to distinct atomic surface arrays, the ensemble effect, and to changes in the electronic structure induced by charge transfer between the metals, the ligand effect. In this work, we present a comprehensive study of carbon-supported PdAu nanoparticles with varying nominal Au content and similar particle sizes. These nanocatalysts were characterized by X-ray diffraction (XRD), transmission electron microscopy (TEM) and X-ray photoelectron spectroscopy (XPS) and their electronic properties were studied by X-ray absorption spectroscopy (XAS) around the Pd L3 edge. Cyclic voltammetry (CV) was used to comparatively evaluate the oxidation/reduction behavior of the carbon-supported PdAu nanoparticles as well as the oxidation of adsorbed CO and the charges of adsorbed hydrogen. Deeper understanding of the effects that determine these electrochemical processes is essential for developing new and efficient electrocatalysts. To the best of our knowledge, despite the impact that these surface processes taking place on PdAu/C nanocatalysts of different compositions might have on energy-related electrochemical processes, they were not yet analyzed in the context of the changes of electronic properties and/or surface compositions promoted by the variation of Au content.

EXPERIMENTAL SECTION

Synthesis of carbon-supported PdAu nanoparticles. Colloidal PdAu nanoparticles with different Au contents (20 to 50%, in atoms) were synthesized in a two-phase liquid-liquid system²³⁻²⁴ modified by the addition of oleylamine and oleic acid as capping agents and then supported on carbon powder (Vulcan XC-72, Cabot Corp.). Initially, the two-phase system was prepared by mixing an aqueous solution of the metal precursors (PdCl₂ and HAuCl₄·3H₂O) with a solution containing 0.26 g of a phase-transfer agent (tetraoctylammonium bromide - ToABr) in 17.8 mL of toluene. The molar ratio ToABr:metal was 2.35:1. The two-phase system was then kept under magnetic stirring for 2 hours in order to allow the metallic complex to be transferred from the aqueous solution to the organic phase. When this transfer process was completed, the aqueous phase changed from a reddish color to transparency. In sequence, oleylamine (36.9 μL) and oleic acid (18.8 μL) were added to the system in a molar ratio in relation to metals of 0.84:1 and 0.6:1, respectively. After 10 minutes of magnetic stirring for proper mixing of the capping agents, the metal reduction process was carried out through a drop by drop addition of cooled solution of NaBH₄ 0.2M (5 °C) until the reducer to metal molar ratio was of 10:1. This reduction step was done with the system in an ice bath in order to slow down Au reduction. After that, the system was left under magnetic stirring for another 11 hours and then the water phase was discarded. (The procedure is illustrated in Figure S1, Supporting information).

Carbon powder in amount to get catalysts with a metal loading of 20 wt.% was added to the colloidal suspension of nanoparticles in the organic phase, which was maintained under stirring for 12 hours. The carbon-supported PdAu nanoparticles were then filtered and wash with ethanol, acetone and water. After this initial washing, the PdAu/C sample was dispersed in a solution of KOH in ethanol (0.1 M). The dispersion was maintained in an ultrasonic bath for 20 min, filtered

and washed again with ethanol, acetone and water. This procedure (dispersion, filtering and washing) was done twice. Finally, the catalysts were dried for 2 hours at 80°C. For the sake of simplicity, the materials will be denominated using their nominal atomic composition: Pd₈₀Au₂₀/C, Pd₇₀Au₃₀/C, Pd₆₀Au₄₀/C and Pd₅₀Au₅₀/C.

Catalysts characterization. XRD measurements were performed with a Rigaku DMax 2500 PC diffractometer at scan rate of 1° min⁻¹ in the 2θ range 20–100° and using radiation of 1.5406 Å wavelength (Cu Kα). Transmission electron microscopy images were obtained in a JEOL JEM2100 LaB₆ instrument operating at 200 keV. Some images were taken in scanning mode (STEM) in a FEI TECNAI G2 F20 HRTEM microscope. The samples for TEM and STEM analysis were prepared by placing a drop of a suspension of catalyst in ethanol onto a carbon-coated copper grid that was left to dry in air.

The electronic properties were studied by X-ray absorption spectroscopy (XAS) at the Tender X-rays spectroscopy beamline of the Brazilian Synchrotron Light Laboratory (LNLS). Absorption spectra around the Pd L₃ edge (3173 eV) were measured in total electron yield mode (TEY), with resolution of 2.2 eV, as described elsewhere.²⁵ All spectra were normalized with the ATHENA program²⁶. X-ray photoelectron spectroscopy (XPS) analysis was carried out using monochromatic Al Kα (1486.7 eV) as photon source. All the spectra were collected with the same parameters. In all cases, a 30 eV pass energy was used. For spectra deconvolution, an Au/C sample was analyzed first in order to estimate the instrumental broadening. This value was then used for all other samples. In all cases, a Shirley background was subtracted and all spectra were corrected using C1s core-line (284.5 eV) as reference. A Lorentzian function was used for all non-metallic components. An asymmetric function was used for all metallic components to take into account the interaction between the positive hole created by the photoemission with the conduction

electrons near the Fermi level.²⁷⁻²⁸ The asymmetric function used is a convolution of two Lorentzian (L) functions with different full width at half maximum (FWHM). The Lorentzian function has $\text{FWHM}_1 = w_1$ when the binding energy (BE) is below the peak center (BE_p), *i.e.*, for $\text{BE} < \text{BE}_p$, and has $\text{FWHM}_2 = w_2$ when $\text{BE} > \text{BE}_p$.

Electrochemical measurements. The experiments were carried out in a conventional three-compartment electrochemical cell. For these measurements, the catalysts were used in the form of ultrathin layer. The catalyst ink was prepared with 2.9 mg of catalyst powder, 15 μL of Nafion[®] solution (5 wt.% in a mixture of lower aliphatic alcohols and water) and 1.0 mL of isopropanol. Using a micro-syringe, 13 μL of catalyst ink were deposited on a polished glassy carbon electrode (0.247 cm^2 geometric area), so the metal load on the electrode was 28 $\mu\text{g cm}^{-2}$. A platinum wire and a reversible hydrogen electrode were used as counter and reference electrodes, respectively. Cyclic voltammetry (CV) experiments were carried out in deoxygenated 0.5 M H_2SO_4 solutions at scan rate of 50 mV s^{-1} . For CO oxidation experiments, CO was adsorbed on the surface with the electrode polarized at 0.35 V to avoid interference of adsorbed hydrogen²⁹ and, after removing CO from the solution by bubbling Ar during 15 minutes, it was stripped by sweeping the potential up to 1.0 V at 10 mV s^{-1} . All electrochemical measurements were carried out at room temperature.

RESULTS AND DISCUSSION

Catalysts properties. For all samples, diffraction patterns show a broad peak at around 25° attributed to the [002] planes of carbon with hexagonal structure. The diffraction pattern of Pd/C shows the signals typical of the face centered cubic (fcc) structure of Pd (PDF 87-643) at about 40°, 47°, 68°, 82° and 85°, which correspond to the [111], [200], [220], [311] and [222] planes,

respectively. The PdAu/C samples show patterns similar to that of Pd/C, but with Bragg reflections shifted towards lower values of 2θ . This shift in peak position indicates alloy formation, as partial substitution of Pd by larger Au atoms in the fcc structure produces a lattice expansion. The diffraction patterns obtained for PdAu/C samples, Pd/C and Au/C are shown in Figure S2, Supporting Information.

All calculations from the XRD data were performed using the [220] diffraction peaks because carbon signals do not interfere in this 2θ region. The [220] peak position and the width at half intensity (ω) were obtained by fitting a pseudo-Voigt function. The average crystallite diameter (D) was estimated using Scherrer's equation for spherical particles:

$$D = \frac{0.9\lambda}{\omega \cos \theta} \quad (1)$$

where λ is the wavelength of the X-ray radiation (1.54056 Å) and θ is the angle of the Bragg reflection. The apparent lattice parameter (a)

$$a = \frac{\sqrt{2}\lambda}{\sin \theta} \quad (2)$$

and the average Pd-Pd distance (d_{fcc})

$$d_{\text{fcc}} = \frac{\sqrt{2}}{2} a \quad (3)$$

at the [220] diffraction³⁰ were also calculated. Results are summarized on Table 1. The apparent lattice parameter of Pd/C (3.912 Å) was found to be somewhat larger than the value for Pd metal (3.890 Å). This cell expansion can be ascribed to lattice strain,³⁰ which is frequently observed for nanoparticles and it has been reported for Pd,^{6, 25, 31} Ag,³² Au and Pt.³³ Differently, the lattice parameter calculated for Au/C (4.076 Å) is in good agreement with that of pure Au (4.078 Å). The

lattice parameter for PdAu/C catalysts generally increases with Au content indicating alloy formation. The composition of the PdAu alloyed phase can be estimated from Vegard's law: ³⁰

$$a_{\text{alloy}} = a_{\text{Pd}}(1 - x_{\text{Au}}) + a_{\text{Au}} x_{\text{Au}} \quad (4)$$

where a_{alloy} is the apparent lattice parameter of the PdAu solid solutions, a_{Pd} is the lattice parameter of the Pd/C sample (3.912 Å), a_{Au} is the lattice parameter of Au/C (4.076 Å) and x_{Au} is the molar fraction of Au in the PdAu alloy. The results are shown in Table 1 and indicate that the PdAu alloyed phases are richer in Au as compared with the nominal compositions, suggesting that some segregation occurs.

Table 1. Structural properties of house-made PdAu/C, Pd/C and Au/C samples derived from XRD characterization and average particle diameter from STEM images.

Sample	Crystallite size (nm)	Lattice Constant (Å)	Pd-Pd distance (Å)	Pd:Au (alloyed)	Particle size (nm)
Pd/C	2.1	3.912	2.766	-	4.1 ± 1.0
Pd ₈₀ Au ₂₀ /C	2.5	3.985	2,818	55:45	5.2 ± 1.1
Pd ₇₀ Au ₃₀ /C	2.5	3.993	2.823	51:49	4.0 ± 1.1
Pd ₆₀ Au ₄₀ /C	2.5	4.012	2.837	39:61	2.9 ± 0.6
Pd ₅₀ Au ₅₀ /C	2.3	4.006	2.834	41:59	3.3 ± 0.6
Au/C	8.91	4.076	–	–	–

Figure 1 shows STEM images for Pd₅₀Au₅₀/C where we can see that nanoparticles are well dispersed on the carbon support. Average particle sizes obtained from size distribution histograms

are given in Table 1. (Other images and the size distribution histograms for PdAu/C catalysts are shown in Figures S3 and S4, Supporting Information).

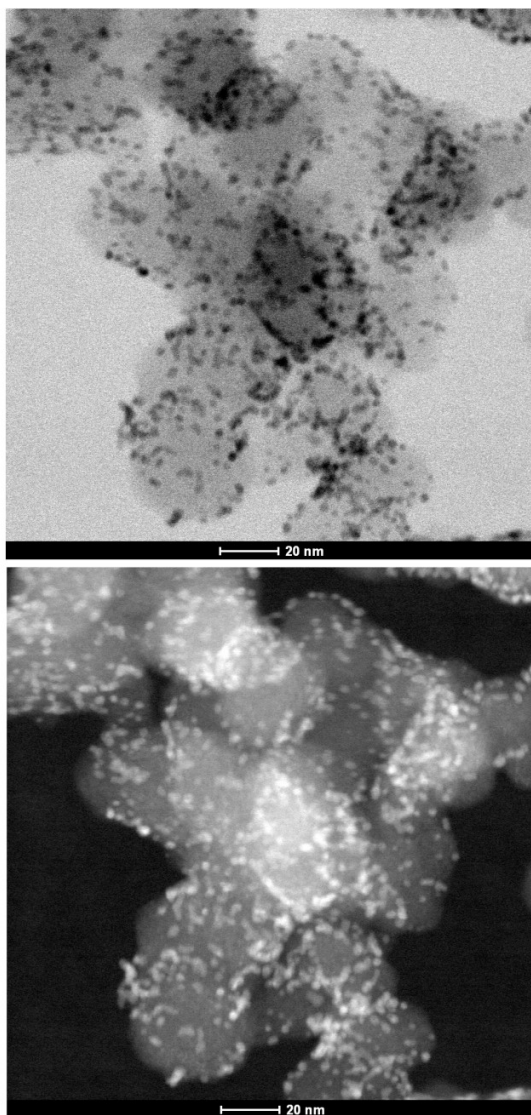


Figure 1. Bright and dark field STEM images of Pd₅₀Au₅₀/C.

Consensus regarding rehybridization and small net charge transfer from Pd to Au seems to have been reached, supported by data from several techniques such as XPS³⁴⁻³⁷ and a smaller number of results from X-ray absorption spectroscopy, mostly from experiments around the Pd K-edge

(24350.3 eV) and the Au L3 edge (11918.7 eV).^{35,38-43} In this work, X-ray absorption spectroscopy (XAS) experiments were carried out around the Pd L3 edge (3173 eV) to investigate the Pd electronic structure. Absorption at the Pd L3 edge promotes the excitation of 2p electrons to vacant d orbitals ($2p_{3/2} \rightarrow 4d$). Consequently, lower X-ray absorption would be measured if the Pd 4d orbitals are more filled and higher if they are more empty.⁴⁴ Accordingly, these measurements allow comparing the electronic occupation of the Pd 4d band, which is the relevant one in chemisorption processes. The shift in the Pd d-band center promoted by the changes in the electronic occupancy of the Pd 4d band might dramatically alter the way in which Pd interacts with adsorbates.⁴⁵

XAS spectra measured around the Pd L3 edge for Pd/C and PdAu/C samples are shown in Figure 2a. A small signal associated to the Au M2 edge (3148 eV) is observed for all PdAu samples in the pre-edge region of Pd L3 (*c.a.* -25 eV), indicating the presence of Au on the surface of the particles.

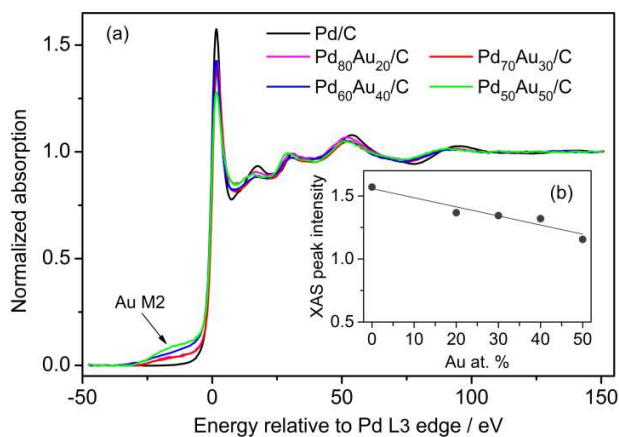


Figure 2. (a) Normalized X-ray absorption spectra of PdAu/C and Pd/C catalysts. (b) Intensity of the L3 absorption peak against nominal Au content.

The spectra of Figure 2a also show that the intensity of the absorption peak for all PdAu/C samples is lower than for Pd/C, indicating a larger electronic occupancy of the Pd 4d band. The peak absorption intensity, after discounting the contribution due to the absorption of Au, allows comparing qualitatively the Pd 4d band electronic occupancy. As shown in Figure 2b, the Pd 4d band is less empty as the content of Au increases.

XPS Pd 3d and Au 4f spectra are shown in Figures 3 and 4, respectively. The spectrum of the Pd/C sample was deconvoluted using one component corresponding to Pd⁰ and two components corresponding to oxidized states (Pd-Ox₁ and Pd-Ox₂). The Au 4f spectra were deconvoluted using two contributions arising from Au⁰ and Auⁿ⁺. This last one is probably due to exposure to the atmosphere. Also, a third contribution due to Pd 4s was included. All the parameters were left to vary freely. The obtained values for the spin-orbit splitting and area ratio of the Pd 3d and Au 4f core-lines are in excellent agreement with the expected values.⁴⁶ The obtained binding energies of the Pd⁰ component and the Au⁰ component, 335.5 eV for Pd/C and 84.2 eV for Au/C, are in good agreement with the reported values.⁴⁶⁻⁴⁷ The slightly higher BE has been shown to be due to small particle size.⁴⁸ The results of the deconvolution are summarized in Table S1, Supporting Information. The Pd-Ox₁ and Pd-Ox₂ species can be attributed to different palladium oxide phases. The assignment to a specific palladium oxide structure for each component is rather challenging, because different binding energy values for each oxide type are found in the literature.^{47, 49-53} However, the component with the highest binding energy (*c.a.* 337.5 eV) is commonly assigned to bulk PdO^{50, 52-53} while the component at intermediate binding energy values (*c.a.* 336 eV) can be assigned to a surface-like oxide or PdO oxide in contact with metallic Pd.^{49, 52-53} For the PdAu/C materials (Figure 3), a component from Au 4d_{5/2} was also included for deconvolution.

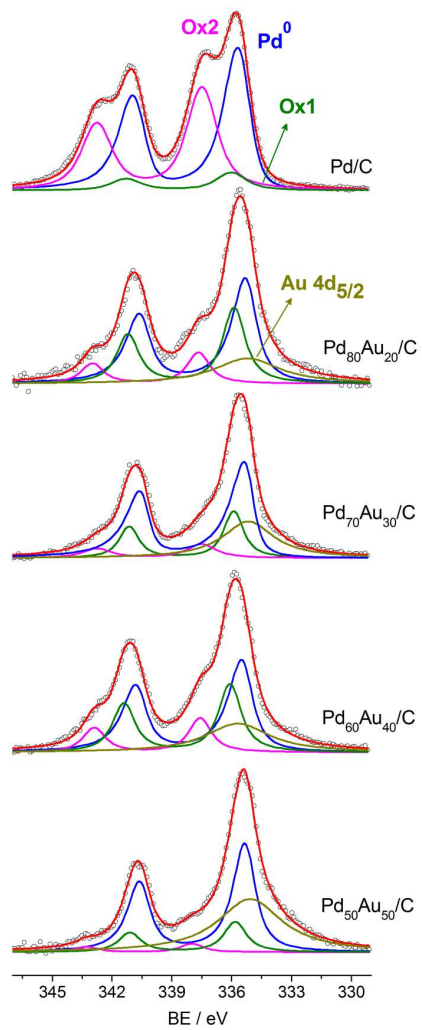


Figure 3. XPS Pd 3d spectra for Pd/C and PdAu/C samples and deconvolutions using three components for Pd oxidation states and a component from Au 4d_{5/2}.

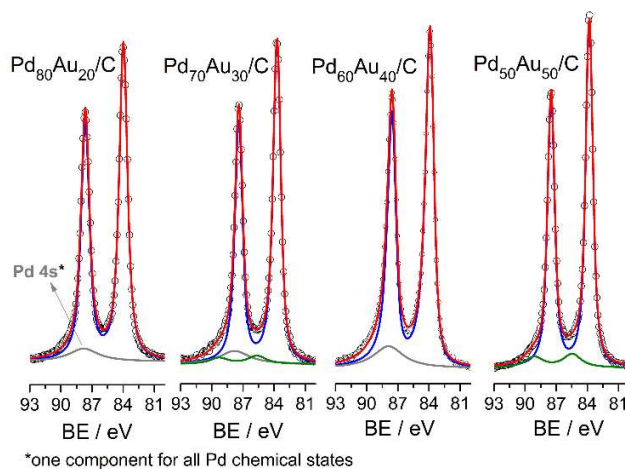


Figure 4. XPS Au 4f spectra for PdAu/C samples and deconvolutions. Blue line for Au⁰ and green line for Auⁿ⁺ components.

The results from the data analysis are depicted in Figure 5. It can be seen that the composition of the Pd oxide phase changes with the Au content (Figure 5a). The presence of Au decreases the amount of bulk-like Pd oxide (PdOx₂ component). Also, as the Au content increases the total amount of Pd oxide decreases leading to more metallic content (Figure 5b). It is important to note here that the decrease in the bulk-like Pd oxide (PdOx₂) amount for increasing Au content is consistent with the increase in the Pd 4d band electronic occupancy, as evidenced by XAS data. DFT calculations show a linear correlation of the oxygen adsorption energies and the d-band position of Pd atoms on other metal surfaces.⁵⁴ The downshift of the d-band center of Pd “skin” materials (consequence of the higher filling of the d-band) decreases the adsorption energy of oxygen thus, making the interaction between oxygen and palladium weaker.⁵⁴

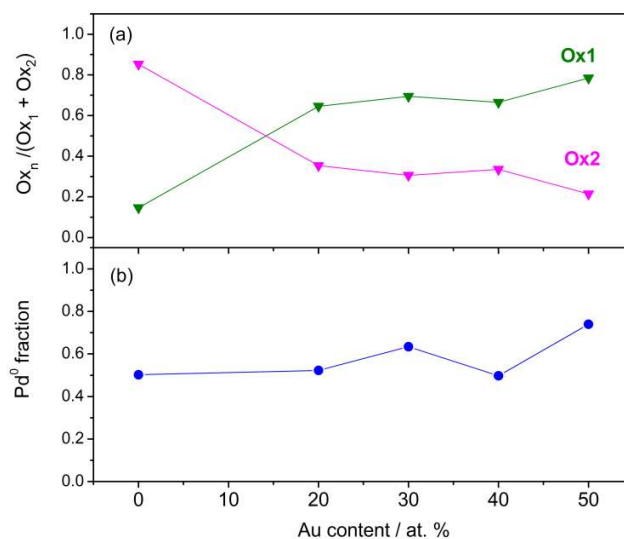


Figure 5. (a) Pd oxide phase components Ox1 (surface-like) and Ox2 (bulk-like) against nominal Au content. (b) Fraction of metallic Pd against nominal Au content.

For the PdAu/C materials the BE of Pd 3d and Au 4f shift both to lower values with respect to the pure elements (see Table S1, Supporting Information). This core level shift (CLS) has been already observed for PdAu alloys.^{13, 55-56} It has been reported that the net charge flowing into Au may result in a CLS of Au 4f as high as -0.4 eV, and that Pd 3d shows a CLS of -0.1 eV due to the gain of d electrons from Au.⁵⁵⁻⁵⁶ Data of Table S1 reveal that for the PdAu/C materials a CLS of *c.a.* -0.1 to -0.2 eV and of -0.2 to -0.4 eV is observed for Pd 3d and Au 4f, respectively. This shift in BE is due to the rehybridization and charge redistribution, where Au gains sp electrons, compensated by a loss of d electrons transferred to Pd.^{13, 55-56} Thus, the higher Pd 4d band occupancy observed herein (see Figure 2) is also a consequence of alloying of Pd with Au and not only due to the reduced amount of oxides in the PdAu/C materials. The asymmetry of the Pd⁰ component in Pd 3d of the PdAu/C materials is slightly lower than for pure Pd, in good agreement

with lower asymmetry parameters observed for some Pd-alloys⁵⁷ and in line with a higher Pd 4d band occupancy.⁵⁸

The Au atomic concentrations were estimated using the corresponding photo-ionization cross-sections for 1487 eV photon energy.⁵⁹ Results obtained from Pd 3d and Au 4d signals are summarized in Table 2. (Au contents obtained from Pd 3d and Au 4f signals are given in Table S2, Supporting Information).

Table 2. Au atomic percentage calculated from Pd 3d and Au 4d signals.

Catalyst	Au content (at. %)
Pd ₈₀ Au ₂₀ /C	21.4
Pd ₇₀ Au ₃₀ /C	32.2
Pd ₆₀ Au ₄₀ /C	28.1
Pd ₅₀ Au ₅₀ /C	46.3

The inelastic mean free path (IMFP) of photoelectrons with a kinetic energy (KE) of c.a. 1150 eV (Pd 3d and Au 4f) is approximately 1.3–2 nm⁶⁰ while for photoelectrons with a KE of c.a. 1400 eV (Au 4f), the IMFP is approximately 1.6–2.3 nm.⁶⁰⁻⁶¹ The results indicate that the compositions of the PdAu materials are relatively close to the nominal ones, except for Pd₆₀Au₄₀/C for which is somewhat lower.

With the preceding result in mind, it is worth returning to the results obtained by XRD analysis (Table 1). Since the average size of the PdAu nanoparticles is small (3–5 nm, as seen by TEM), the probing depth of XPS analysis gives in this case information on the composition of the whole

particles and not only the surface. Moreover, atomic composition determined by XPS is obtained considering all the Pd and Au phases, *i.e.* both metallic and oxides. In contrast, although XRD analysis gives bulk information, it only probes crystalline phases. In this case, only the metallic phases since no Bragg reflections corresponding to oxides are observed. However, XPS analysis clearly shows the presence of Pd oxides (and a minor amount of Au oxide). Consequently, the alloyed phase composition estimated from XRD shows an Au-rich phase with composition higher than the nominal composition. One can conclude from the preceding analysis that the nanoparticles have an Au-rich alloyed phase with a Pd-rich surface, which forms Pd oxides upon air exposure.

Electrochemical characterization. CV curves measured in 0.5 M H₂SO₄ solution at 50 mV s⁻¹ recorded in the potential range of 0.05–1.65 V for PdAu/C, Pd/C and Au/C catalysts are shown in Figure 6a.

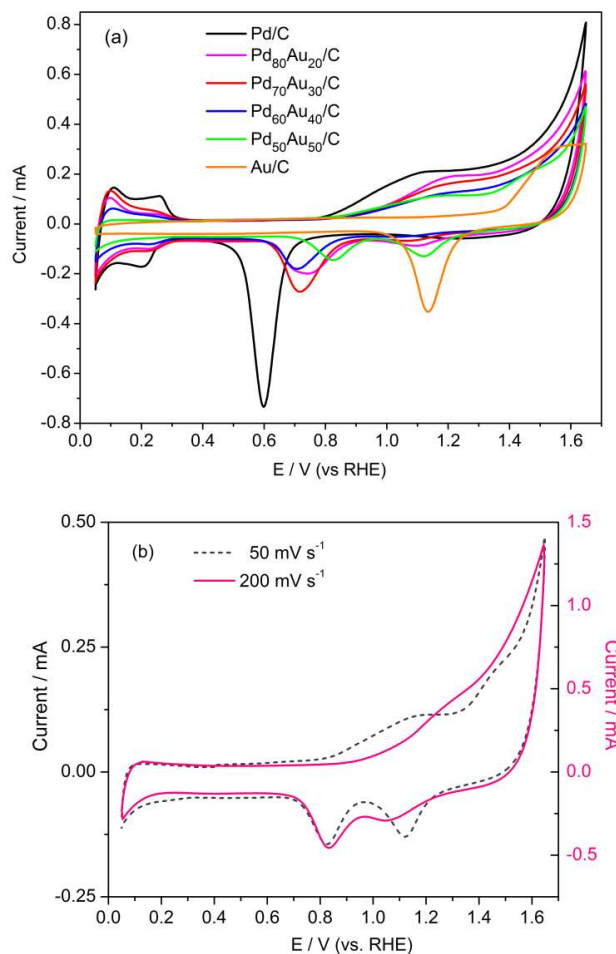


Figure 6. (a) Cyclic voltammetry curves measured in Ar purged 0.5 H₂SO₄ for PdAu/C, Pd/C and Au/C catalysts. Sweep rate: 0.05 V s⁻¹. (b) Comparison of cycle voltammetry curves recorded for Pd₅₀Au₅₀/C at 0.05 and 0.20 V s⁻¹.

In general, all curves show currents associated to metal oxidation/reduction and the hydrogen adsorption/desorption processes over Pd sites between *c.a.* 0.05–0.4 V, which involve a lower charge on PdAu/C materials than on Pd/C. In the positive scan, the surface oxidation is seen above *c.a.* 0.8 V, although the onset of oxidation of PdAu/C samples is shifted towards more positive

potentials. The negative-going sweep shows two reduction waves for PdAu/C catalysts. The first one, which appears in the 1.0–1.2 V potential range, corresponds to the reduction of Au oxides. According to literature, the current peak of reduction of Au oxides develops on PdAu alloys as result of dissolution of Pd taking place during the positive-going scan.⁶² Thus, the Au reduction peak should be smaller at higher sweep rates because dissolution of Pd would decrease and that was indeed observed, as illustrated in Figure 6b for Pd₅₀Au₅₀/C. Current peaks related to the reduction of Pd oxides are observed in the potential range of 0.6–0.9V. All electrodes contained the same amount of metals (Pd + Au = 28 μg cm⁻²), so the apparent variation of the charge involved in the oxide reduction processes would result from the different compositions of PdAu/C samples.

The shift towards higher potentials of the reduction of Pd oxides promoted by Au is a well-known phenomenon and it was studied comprehensively for PdAu alloys by Rand and Woods,⁶² that established that there is linear relation between the composition of the surface alloy and the potential of the reduction peak. Thus, we used the same approach and employed the position of the current peak of Pd oxide reduction to estimate the amounts of metals in the surface alloy. In all cases, the amount of Au was found to be lower than the nominal value. Results are summarized in Table 3. Comparison of the composition of the surface with the one estimated from XRD data for the alloyed phase (Table 1) also suggests that, as compared with the nominal composition, the inner part of the PdAu nanoparticles is richer in Au, while the outermost layers are enriched in Pd.

Table 3. Peak potential of the reduction of Pd oxides (E_p), estimated composition of surface alloy, and upper potential limit (E_{UL}) of completion of a Pd oxide monolayer.

E _p (V)	Pd:Au (surface alloy)	E _{UL} (V)
--------------------	--------------------------	---------------------

Pd/C	0.598	100:0	1.45
Pd ₈₀ Au ₂₀ /C	0.740	73:27	1.58
Pd ₇₀ Au ₃₀ /C	0.718	77:23	1.56
Pd ₆₀ Au ₄₀ /C	0.706	80:20	1.55
Pd ₅₀ Au ₅₀ /C	0.824	58:42	1.65

It is well known for Pd electrodes that the potential of the peak of reduction of Pd oxides depends on the Pd oxidation charge passed on the positive-going potential scan.⁶³ In other words, the reduction peak appearing at higher potentials would indicate a thinner oxide layer. Figure 7 shows a plot of peak potential of Pd oxide reduction against the Pd L3 edge absorption intensity. Noticeably, the potential at which the reduction peak appears is more positive as the Pd 4d band electronic occupation increases. Thus, the shift of the peak potential observed for PdAu/C materials might be consequence of the formation of thinner Pd oxides for growing amounts of Au. Indeed, for PdAu alloys potentiostatically deposited on Au wires, a linear dependence of the upper potential limit (E_{UL}) for completion of a Pd oxide monolayer with Au content was reported.⁶⁴

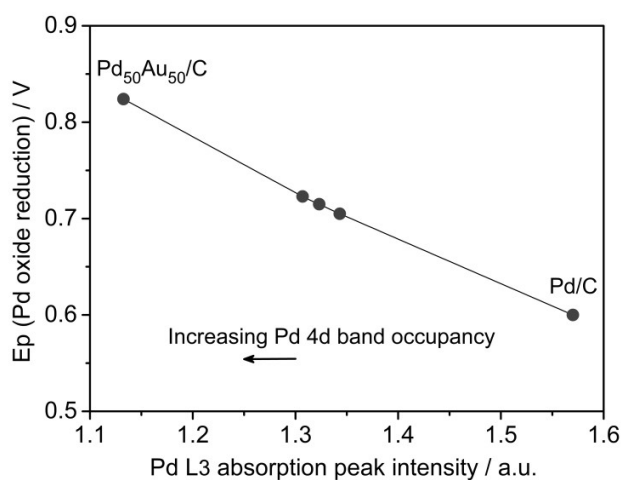


Figure 7. Peak potential of reduction of Pd oxides against the intensity of the absorption peak of XAS spectra measured around the L3 edge depicted in Figure 2.

The electrochemically active area (EAA) of Pd can be calculated from the reduction charge of a Pd oxide monolayer ($424 \mu\text{C cm}^{-2}$).⁶⁵ In acid solution, a monolayer is completed on Pd at *c.a.* 1.45 V,⁶⁴⁻⁶⁸ value that was also reported for carbon-supported Pd nanoparticles.²⁹ In this work, we used the linear relation reported⁶⁴ and estimated the E_{UL} at which a Pd oxide monolayer would be completed for each PdAu/C sample using the surface alloy composition (see Table 2). Then, CV curves were recorded up to the corresponding E_{UL} value to allow calculating the reduction charge of the Pd oxide monolayer.

The EAA of Pd was also estimated from the oxidation of adsorbed CO. Because the charge involved in the CO stripping curve also includes the charge associated to Pd oxidation, to separate one from the other it is usual to subtract the current measured in the absence of CO from the recorded CO stripping curve. On the other hand, the reduction charge after CO oxidation up to 1.0 V can be ascribed only to the reduction of Pd oxide. Therefore, the difference between the anodic (CO oxidation + Pd oxidation) and the cathodic charge (Pd oxide reduction) should, in principle, allow separating the charges associated to each anodic process. Because during the positive-going sweep, Pd dissolution also takes place and it should be accounted for. One way to do that is correcting the PdO reduction charge using the ratio of the anodic to cathodic charge from a CV obtained in a solution without CO between the same potential limits and at the same scan rate. In this way, any effect on the EAA of Pd that might result from irreversible alterations,⁶⁹ and/or surface segregation in the case of alloys,⁷⁰ caused by CO adsorption on surface of nanoparticles should be minimized. The values of Pd EAA derived from PdO reduction charges and from CO

stripping experiments are plotted against the Au content in Figure 8. The good agreement of calculated values indicates that both methods lead to good estimates of Pd EAA. Additionally, the consistency of data depicted in Figure 8 also suggests that, in contrast with what was proposed in the literature,⁶⁸ CO is likely to be mostly linearly bonded with coverage of Pd sites close to 1.

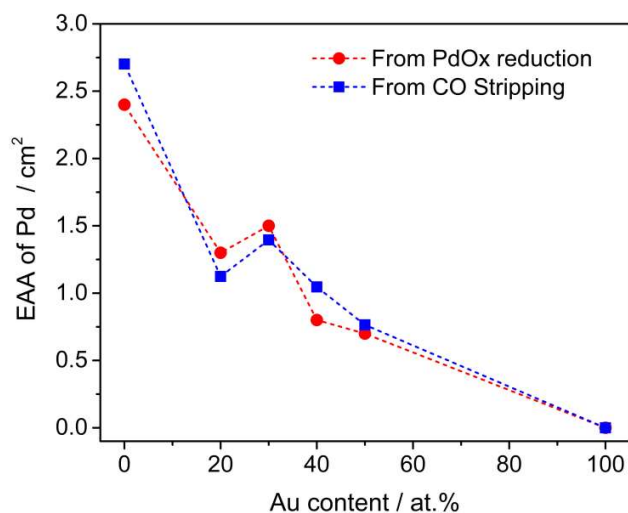


Figure 8. Electrochemically active area (EAA) of Pd calculated from the reduction charge of a Pd oxide monolayer and from adsorbed CO oxidation as a function of Au content.

Measured CO stripping currents were lower on PdAu/C catalysts than on Pd/C, most likely because of the Pd EAA differences, as shown in Figure 9 that also reveals that adsorbed CO oxidation begins at lower potentials, except for Pd₅₀Au₅₀/C. It is also noticed that the sequence of peak potential (Pd₈₀Au₂₀/C < Pd₇₀Au₃₀/C < Pd₆₀Au₄₀/C < Pd/C < Pd₅₀Au₅₀/C) does not follow the trend of electronic occupancy of the Pd 4d band.

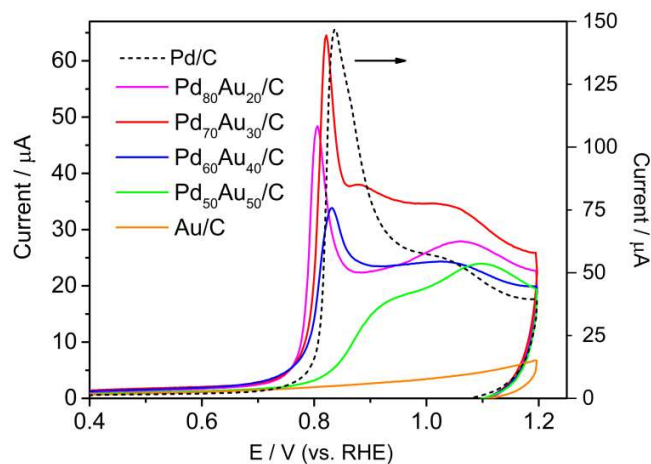


Figure 9. Current-potential curves of oxidation of CO adsorbed on PdAu/C catalysts compared with those for Pd/C and Au/C samples.

Liu and Norskov ⁷¹ performed Density Functional Theory (DFT) calculations for nitrogen, oxygen and CO adsorption on Au/Pd(111) with varying Au content, and suggested that CO binding energies on Au/Pd(111) surfaces would be weaker than on pure Pd, at the time that “mixed” sites would be less favorable for adsorption than “unmixed” Pd sites. That being the case, lower adsorption energies should be expected for the Pd₅₀Au₅₀/C catalyst, which surface composition is much closer to a 1:1 atomic Pd:Au ratio (see Table 2). The CO stripping curves for PdAu/C catalysts depicted in Figure 9, however, show a clear shift towards higher potentials as the nominal Au content increases. This apparent inconsistency can be explained keeping in mind that removal of adsorbed CO through a bifunctional mechanism involves oxygen-containing species, which formation at low potentials is hindered as the Au content increases as evidenced by XPS data and results for the electrochemical formation of Pd oxides discussed above.

The electrochemical adsorption of hydrogen is also an important process because it is the first step in hydrogen evolution in acid solutions. Hydrogen adsorption/desorption charges are also

dependent on Au content. If the charge variation would merely follow the Pd EAA, then the H desorption charge (Q_H) should be close to half the Pd oxide reduction charge (Q_{PdOx}) for all PdAu/C samples. The ratio Q_H/Q_{PdOx} depicted in Figure 10 evidences that for nominal Au content above 30% the value of Q_H is considerably smaller than expected. No correlation with the variation on the d-character of Pd is apparent.

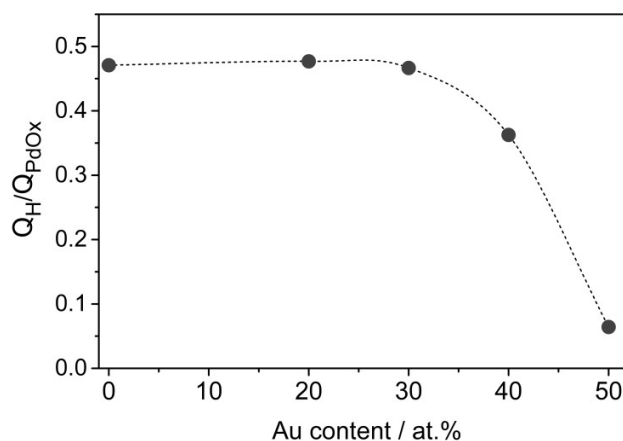


Figure 10. Ratio of hydrogen desorption and Pd oxides reduction charges against Au content.

Ligand and ensemble effects. XAS results show that the addition of Au promotes an increase in the electronic occupation of the Pd 4d band, which is the electronic band involved in the interaction of adsorbates and Pd sites, suggesting that PdAu/C materials behave in a more “Au-like” fashion as the Au content increases. XPS data, on the other hand, indicate that Au promotes an increase in the metallic Pd content while the oxide content shows growing amounts of surface-like Pd-O_{x1} at the expense of bulk-like Pd-O_{x2}. Altogether, these results point out that the more filled Pd 4d band promoted by the presence of Au reduces the tendency of Pd towards oxidation. Consistent with that, CV results showed that the peak potential of reduction of Pd oxide follows well the XAS absorption intensity indicating that thinner layers of Pd oxide are formed as the Au

content increases. That is also supported by the linear relationship between E_{UL} corresponding to completion of a Pd oxide monolayer and the Au content proposed in the literature ⁶⁴ and used above for the calculation of the Pd EAA. In other words, the whole set of results consistently demonstrates that the formation of a Pd oxide layer on PdAu/C catalysts is mainly determined by a ligand effect.

In contrast, the oxidation of adsorbed CO does not follow the same trend of the electronic properties. The lower potentials for CO stripping observed for PdAu/C catalysts with Au contents up to 40% is compatible with lower CO adsorption energies on PdAu as compared to Pd. According to DFT calculations, ensemble effects would then overcome the ligand effect. ⁷¹ Thus, while CO adsorption appears to be mainly governed by ensemble effects its oxidation seems to be affected by the availability of oxygenated species, which is dominated by ligand effects.

The oxidation of the Pd surface is relevant not only for catalytic processes that require oxygenated species to proceed, as the oxidation of adsorbed CO. It is also very important for catalytic reactions where the reactant adsorbs only on oxide-free sites, as is the case of oxygen reduction. The shift towards higher values of the potential of formation of a full monolayer of Pd oxides implies that over the potential region of practical interest for this reaction (*c.a.* 0.7–1.0 V) the fraction of oxide-free Pd sites available for O₂ adsorption would be larger as the Au content increases. Thus, O₂ reduction currents higher on PdAu materials than on pure Pd would be expected, as well as a narrower potential region for coverage of adsorbed oxygen following a Temkin adsorption isotherm.⁷² However, the resulting specific catalytic activity for O₂ reduction (*i.e.* assessed in terms of current density) may also be influenced by ligand and ensemble effects. The electronic properties of the reaction sites might affect the adsorption energies of O₂ and reaction intermediates. The surface arrangement of Pd atoms might influence the ways in which

O₂ adsorbs altering the fraction of hydrogen peroxide formed by the different reaction paths (*i.e.*, O₂ reduction going through two or four electrons paths). Based on our data, it is not surprising to find discrepancies regarding for O₂ reduction activities of PdAu catalysts.^{19,73}

Optimum electronic properties have been frequently invoked to explain a catalytic activity maximum observed for the electrochemical oxidation of formic acid on PdAu materials with different Au contents.^{74, 75} The results reported here show that the formation of adsorbed oxygenated species, often considered to inhibit formic acid oxidation by blocking adsorption sites but necessary to remove CO, is not independent of the electronic properties. Thus, combined ligand effects with different coverages of adsorbed oxygen-containing species is a more likely explanation of that kind of results.

The charge of oxidation of adsorbed H, which is also largely influenced by the Au content, does not seem to be determined by the electronic properties, suggesting that the adsorption of hydrogen is determined predominantly by ensemble effects. As mentioned above, H adsorption is the first step of H₂ evolution, which takes place in the same potential region than the electrochemical reduction of CO₂. Our results might be helpful for improving the catalysis of CO₂ reduction on PdAu materials⁷⁷ by decreasing the faradaic efficiency of H₂ evolution.

CONCLUSIONS

We have studied a set of PdAu/C samples of different compositions that were all prepared by the same procedure and have similar average particle diameters. XRD combined with XPS results suggest that the surface of PdAu nanoparticles is enriched in Pd while the inner part is richer in Au. The electronic occupation of the Pd 4d band was assessed from X-ray absorption measurements around the Pd L3 edge, which evidences “d” electron density donation from Au to

Pd. In good agreement with that, XPS results evidence that the presence of Au promotes an increase in the Pd metallic content accompanied by an increase in the content of surface-like Pd oxide at the expense of the bulk-like oxide species. We also showed that evaluating of the surface alloy composition from the peak potential of Pd oxide reduction and using it to estimate the value of E_{UL} for completion of a Pd oxide monolayer allows calculating the Pd EAA values from the reduction charges, which are in very good agreement with those derived from CO stripping data. Moreover, the estimated compositions of the surface alloy also indicate Pd-enriched surfaces, as compared with nominal compositions. Altogether, results evidence that in acid solution the formation of a Pd oxide layer on PdAu/C catalysts is governed by the electronic occupancy of the Pd 4d band (ligand effects). Instead, ensemble effects determine the adsorption of hydrogen. For adsorbed CO oxidation, the shift towards lower potentials verified for PdAu/C catalysts with low Au contents, as compared to Pd/C, indicates that ensemble effects determine the CO binding strength. On the other hand, the increase in Au content produces a gradual positive shift that reveals the effects of the availability of oxygenated species, which depends on the electronic properties. Overall, these findings reveal that different electrochemical surface processes taking place on PdAu/C nanocatalysts are influenced in different extents by the atomic surface arrays and electronic properties. This offers new rationales to explore profitably ligand and ensemble effects in developing catalysts with good performances towards fuel cell and energy-related reactions.

ACKNOWLEDGMENT. This work was supported by Fundação de Amparo à Pesquisa do Estado de São Paulo (FAPESP) (2014/12255-6), and Conselho Nacional de Desenvolvimento Científico e Tecnológico (CNPq), (407143/2013-0). Thanks are due to the Brazilian Synchrotron Light Laboratory (LNLS) for assisting XAS experiments and to the Brazilian Nanotechnology

National Laboratory (LNNano) for XPS measurements. IBCG thanks CNPq (142497/2013-4) for the fellowships granted.

REFERENCES

1. Singh, A. K.; Xu, Q., *ChemCatChem* **2013**, *5*, 652–676.
2. Long, N. V.; Yang, Y.; Thi, C. M.; Minh, N. V.; Cao, Y. Q.; Nogami, M., *Nano Energy* **2013**, *2*, 636–676.
3. Liu, Z. M.; Ma, L. L.; Zhang, J.; Hongsirikarn, K.; Goodwin, J. G., *Catal. Rev.: Sci. Eng.* **2013**, *55*, 255–288.
4. Shao, M. H.; Chang, Q. W.; Dodelet, J. P.; Chenitz, R., *Chem. Rev.* **2016**, *116*, 3594–3657.
5. Zhang, L. L.; Chang, Q. W.; Chen, H. M.; Shao, M. H., *Nano Energy* **2016**, *29*, 198–219.
6. Pires, F. I.; Villullas, H. M., *Int. J. Hydrogen Energy* **2012**, *37*, 17052–17059.
7. Erikson, H.; Sarapuu, A.; Solla-Gullon, J.; Tammeveski, K., *J. Electroanal. Chem.* **2016**, *780*, 327–336.
8. Zhang, J.; Sasaki, K.; Sutter, E.; Adzic, R. R., *Science* **2007**, *315*, 220–222.
9. Seraj, S.; Kunal, P.; Li, H.; Henkelman, G.; Humphrey, S. M.; Werth, C. J., *ACS Catal.* **2017**, *7*, 3268–3276.

10. Corbos, E. C.; Ellis, P. R.; Cookson, J.; Briois, V.; Hyde, T. I.; Sankar, G.; Bishop, P. T., *Catal. Technol.* **2013**, 3, 2934–2943.
11. Alshammari, A.; Kalevaru, V. N.; Martin, A., *Catalysts* **2016**, 6, 97 DOI: 10.3390/catal6070097.
12. Biasi, P.; Menegazzo, F.; Pinna, F.; Eranen, K.; Salmi, T. O.; Canu, P., *Chem. Eng. J.* **2011**, 176, 172–177.
13. Marx, S.; Baiker, A., *J. Phys. Chem. C* **2009**, 113, 6191–6201.
14. Al-Odail, F. A.; Anastasopoulos, A.; Hayden, B. E., *Phys. Chem. Chem. Phys.* **2010**, 12, 11398–11406.
15. Zhang, Q. L.; Feng, J. X.; Wang, A. J.; Wei, J.; Feng, J. J., *RSC Adv.* **2014**, 4, 52640–52646.
16. Yan, W.; Tang, Z. H.; Wang, L. K.; Wang, Q. N.; Yang, H. Y.; Chen, S. W., *Int. J. Hydrogen Energy* **2017**, 42, 218–227.
17. Lv, J. J.; Li, S. S.; Wang, A. J.; Mei, L. P.; Chen, J. R.; Feng, J. J., *Electrochim. Acta* **2014**, 136, 521–528.
18. Zheng, J. N.; Li, S. S.; Ma, X.; Chen, F. Y.; Wang, A. J.; Chen, J. R.; Feng, J. J., *J. Power Sources* **2014**, 262, 270–278.
19. Erikson, H.; Sarapuu, A.; Kozlova, J.; Matisen, L.; Sammelselg, V.; Tammeveski, K., *Electrocatalysis* **2015**, 6, 77–85.
20. Suo, Y. G.; Hsing, I. M., *Electrochim. Acta* **2011**, 56, 2174–2183.

21. Wang, H.; Ge, X. B., *Electroanalysis* **2012**, 24, 911–916.
22. Schmidt, T. J.; Jusys, Z.; Gasteiger, H. A.; Behm, R. J.; Endruschat, U.; Boennemann, H., *J. Electroanal. Chem.* **2001**, 501, 132–140.
23. Brust, M.; Walker, M.; Bethell, D.; Schiffrin, D. J.; Whyman, R., *J. Chem. Soc., Chem. Commun.* **1994**, 801–802.
24. Leff, D. V.; Brandt, L.; Heath, J. R., *Langmuir* **1996**, 12, 4723–4730.
25. Alvarenga, G. M.; Gallo, I. B. C.; Villullas, H. M., *J. Catal.* **2017**, 348, 1–8.
26. Ravel, B.; Newville, M., *J. Synchrotron Radiat.* **2005**, 12, 537–541.
27. Hüfner, S., *Photoelectron Spectroscopy. Principles and Applications*. Springer Verlag: Berlin, 2003.
28. Doniach, S.; Sunjic, M., *J. Phys. C: Solid State Phys.* **1970**, 3, 285–291.
29. Lukaszewski, M.; Soszko, M.; Czerwinski, A., *Int. J. Electrochem. Sci.* **2016**, 11, 4442–4469.
30. Cullity, B. C., *Elements of X-ray Diffraction*. second ed.; Addison-Wesley Publishing Company, Inc.: London, 1978.
31. Ohba, T.; Kubo, H.; Ohshima, Y.; Makita, Y.; Nakamura, N.; Uehara, H.; Takakusagi, S.; Asakura, K., *Chem. Lett.* **2015**, 44, 803–805.
32. Wasserman, H. J.; Vermaak, J. S., *Surf. Sci.* **1970**, 22, 164–172.

33. Solliard, C.; Flueli, M., *Surf. Sci.* **1985**, 156, 487–494.
34. Yi, C. W.; Luo, K.; Wei, T.; Goodman, D. W., *J. Phys. Chem. B* **2005**, 109, 18535–18540.
35. Lee, Y. S.; Jeon, Y.; Chung, Y. D.; Lim, K. Y.; Whang, C. N.; Oh, S. J., *J. Korean Phys. Soc.* **2000**, 37, 451–455.
36. Pawelec, B.; Venezia, A. M.; La Parola, V.; Cano-Serrano, E.; Campos-Martin, J. M.; Fierro, J. L. G., *Appl. Surf. Sci.* **2005**, 242, 380–391.
37. Han, Y. F.; Zhong, Z. Y.; Ramesh, K.; Chen, F. X.; Chen, L. W.; White, T.; Tay, Q. L.; Yaakub, S. N.; Wang, Z., *J. Phys. Chem. C* **2007**, 111, 8410–8413.
38. Davis, R. J.; Boudart, M., *J. Phys. Chem.* **1994**, 98, 5471–5477.
39. Couves, J. W.; Meehan, P., *Phys. B* **1995**, 208, 665–667.
40. Oxford, S. M.; Lee, P. L.; Chupas, P. J.; Chapman, K. W.; Kung, M. C.; Kung, H. H., *J. Phys. Chem. C* **2010**, 114, 17085–17091.
41. Verma, P.; Kuwahara, Y.; Mori, K.; Yamashita, H., *J. Mater. Chem. A* **2016**, 4, 10142–10150.
42. Dash, P.; Bond, T.; Fowler, C.; Hou, W.; Coombs, N.; Scott, R. W. J., *J. Phys. Chem. C* **2009**, 113, 12719–12730.
43. Fang, Y.-L.; Miller, J. T.; Guo, N.; Heck, K. N.; Alvarez, P. J. J.; Wong, M. S., *Catal. Today* **2011**, 160, 96–102.

44. Shukla, A. K.; Raman, R. K.; Choudhury, N. A.; Priolkar, K. R.; Sarode, P. R.; Emura, S.; Kumashiro, R., *J. Electroanal. Chem.* **2004**, 563, 181–190.
45. Lima, F. H. B.; Zhang, J.; Shao, M. H.; Sasaki, K.; Vukmirovic, M. B.; Ticianelli, E. A.; Adzic, R. R., *J. Phy. Chem. C* **2007**, 111, 404–410.
46. Moulder, J. F.; Stickle, W. F.; Sobol, P. E.; Bomben, K. D., *Handbook of X Ray Photoelectron Spectroscopy: A Reference Book of Standard Spectra for Identification and Interpretation of XPS Data*. Perkin-Elmer Corporation: USA, 1995.
47. Militello, M. C.; Simko, S. J., *Surf. Sci. Spectra* **1994**, 3, 387–394.
48. Lim, D. C.; Lopez-Salido, I.; Dietsche, R.; Bubek, M.; Kim, Y. D., *Chem. Phys.* **2006**, 330, 441–448.
49. Gabasch, H.; Unterberger, W.; Hayek, K.; Klotzer, B.; Kleimenov, E.; Teschner, D.; Zafeiratos, S.; Havecker, M.; Knop-Gericke, A.; Schlögl, R.; Han, J. Y.; Ribeiro, F. H.; Aszalos-Kiss, B.; Curtin, T.; Zemlyanov, D., *Surf. Sci.* **2006**, 600, 2980–2989.
50. Militello, M. C.; Simko, S. J., *Surf. Sci. Spectra* **1994**, 3, 395–401.
51. Pillo, T.; Zimmermann, R.; Steiner, P.; Hufner, S., *J. Phys.:Condens. Matter* **1997**, 9, 3987–3999.
52. Peuckert, M., *J. Phys. Chem.* **1985**, 89, 2481–2486.
53. Voogt, E. H.; Mens, A. J. M.; Gijzeman, O. L. J.; Geus, J. W., *Surf. Sci.* **1996**, 350, 21–31.

54. Shao, M. H.; Huang, T.; Liu, P.; Zhang, J.; Sasaki, K.; Vukmirovic, M. B.; Adzic, R. R., *Langmuir* **2006**, 22, 10409–10415.
55. Chou, T. S.; Perlman, M. L.; Watson, R. E., *Phys. Rev. B* **1976**, 14, 3248–3250.
56. Nascente, P. A. P.; Decastro, S. G. C.; Landers, R.; Kleiman, G. G., *Phys. Rev. B* **1991**, 43, 4659–4666.
57. Hufner, S.; Wertheim, G. K.; Wernick, J. H., *Solid State Commun.* **1975**, 17, 417–422.
58. *Metallic Alloys: Experimental and Theoretical Perspectives*. Faulkner, J.S.; Jordan, R.G.; Eds.; Springer Netherlands, 1994.
59. Scofield, J. H., *J. Electron Spectrosc. Relat. Phenom.* **1976**, 8, 129–137.
60. Tanuma, S.; Powell, C. J.; Penn, D. R., *Surf. Interface Anal.* **1991**, 17, 911–926.
61. Powell, C. J.; Jablonski, A., *J. Phy. Chem. Ref. Data* **1999**, 28, 19–62.
62. Rand, D. A. J.; Woods, R., *J. Electroanal. Chem.* **1972**, 36, 57–69.
63. Bolzan, A. E.; Martins, M. E.; Arvia, A. J., *J. Electroanal. Chem.* **1983**, 157, 339–358.
64. Lukaszewski, M.; Czerwinski, A., *J. Solid State Electrochem.* **2008**, 12, 1589–1598.
65. Rand, D. A. J.; Woods, R., *J. Electroanal. Chem. Interfacial Electrochem.* **1971**, 31, 29–38.
66. Burshtein, R. K.; Tarasevich, M. R.; Vilinskaya, V. S., *Elektrokhimiya* **1967**, 3, 349–355.
67. Grden, M.; Lukaszewski, M.; Jerkiewicz, G.; Czerwinski, A., *Electrochim. Acta* **2008**, 53, 7583–7598.

68. Fang, L. L.; Tao, Q. A.; Li, M. F.; Liao, L. W.; Chen, D.; Chen, Y. X., *Chin. J. Chem. Phys.* **2010**, *23*, 543–548.
69. Chen, D.; Tao, Q.; Liao, L. W.; Liu, S. X.; Chen, Y. X.; Ye, S., *Electrocatalysis* **2011**, *2*, 207–219.
70. Wang, D. L.; Liu, S. F.; Wang, J.; Lin, R. Q.; Kawasaki, M.; Rus, E.; Silberstein, K. E.; Lowe, M. A.; Lin, F.; Nordlund, D.; Liu, H. F.; Muller, D. A.; Xin, H. L. L.; Abruna, H. D., *Nat. Commun.* **2016**, *7*, 11941 DOI: 10.1038/ncomms11941.
71. Liu, P.; Norskov, J. K., *Phys. Chem. Chem. Phys.* **2001**, *3*, 3814–3818.
72. Tarasevich, M.R.; Sadkovsky, A.; Yeager, E. *Comprehensive treatise of electrochemistry*, vol. 7. New York: Plenum Publishing Corp; 1983.
73. Pizzutilo, E.; Kasian, O.; Choi, C.H.; Cherevko, S.; Hutchings, G.J.; Mayrhofer, K.J.J.; Freakley, S.J. *Chem. Phys. Lett.* **2017**, *683*, 436–442.
74. Hsu, C.; Huang, C.; Hao, Y.; Liu, F. *Electrochem. Commun.* **2012**, *23*, 133–136.
75. Szumelda, T.; Drelinkiewicz, A.; Lalik, E.; Kosydar, R.; Duraczyńska, D.; Gurgul, J. *Appl. Catal. B* **2018**, *221*, 393–405.
76. Plana, D.; Florez-Montano, J.; Celorrio, V.; Pastor E.; Fermin, D. J. *Chem. Commun.*, **2013**, *49*, 10962–10964.

